Journal of Polymers and the Environment (2023) 31:754–767
https://doi.org/10.1007/s10924-022-02544-9

ORIGINAL PAPER

Elongated soy protein isolate-poly(D, L-lactide-co-glycolic acid) microcapsules prepared using syringe filters and their effect on self-healing efficiency of soy protein-based green resin

Shanshan Shi[1] · **Anil N. Netravali**[1]

Accepted: 28 July 2022 / Published online: 4 November 2022

Abstract
Self-healing soy-based resins with soy protein isolate (SPI) containing poly(D, L-lactide-co-glycolic acid) (PLGA) microcapsules (MCs) were prepared. Spherical (diameter of 1.30 μm) and elongated MCs (aspect ratios up to 20) were produced using a membrane emulsification technique using syringe filters. Self-healing efficiencies of resins were characterized for their strength recovery and toughness recovery. While both MCs could successfully heal cracks, spherical MCs were seen to compromise the tensile properties of the resin, whereas elongated MCs demonstrated some mechanical enhancement. For resins with elongated MCs, self-healing efficiencies of about 45% and 41% in terms of strength recovery and toughness recovery, respectively, were obtained. For spherical MCs, the self-healing efficiencies were even higher. However, these higher efficiencies were a result of the compromised tensile properties of the resin. The results also showed that higher MC loading results in higher self-healing efficiency. Use of self-healing green resins can extend the useful life of green composites as well as enhance their safety, thus, allowing them to replace currently used petroleum-based composites in many applications.

Keywords Self-healing · membrane-emulsification · elongated microcapsules · green resin · soy protein

Introduction

Depleting fossil fuels, rapidly changing climate, and the accumulation of petroleum-based plastic waste have raised significant concerns around the world. Efforts to explore and deploy green substitutes, primarily derived from sustainable and yearly renewable biomass, have grown in the past couple of decades at a rapid pace worldwide [1]. Plant-based soy protein has been considered one of the leading green raw material resources because of its worldwide availability and moderate price. Soy protein isolate (SPI), containing about 92% protein, is commercially available [2]. SPI exhibits high solubility in water facilitating green processing. It has also been shown to degrade quickly when exposed to compost medium, eliminating the need for landfills. These characteristics make SPI an excellent raw material for plastics [2]. Incorporating self-healing characteristics in green resins and composites made using them would not only maximize their durability and lower maintenance costs but also improve their safety and promote further sustainability. The field of green materials still being in its infancy, very little research has been carried out on their self-healing characteristics [3]. Kim and Netravali successfully prepared SPI resins [4] and starch resins [5] with (SPI)-containing poly(D, L-lactide-co-glycolic acid) (PLGA) microcapsules (MCs) that demonstrated good self-healing properties.

The spherical MC-based self-healing system was the first self-healing system developed. It is also one of the most successful self-healing systems that can autonomously restore the mechanical properties of polymeric resins [6]. Emulsification has played a crucial role in the microencapsulation of the healants. A wide array of emulsification methods including membrane emulsification [7], high-pressure homogenization [8], ultrasound emulsification [9], and the application of copolymer [10], have been commonly used. Kim and Netravali prepared SPI-PLGA MCs using

✉ Anil N. Netravali
ann2@cornell.edu

[1] Fiber Science and Apparel Design, Cornell University, 14853-4401 Ithaca, NY, USA

high-pressure homogenization to build a water-in-oil-in-water (W/O/W) emulsion system and embedded them into the SPI composites [4]. Their results showed composites with about 30% self-healing efficiency. Compared to high-pressure homogenization, membrane emulsification has been favored because it can produce MCs with tunable sizes, high encapsulation efficiency, and minimum degradation of entrapped components [7]. Various membranes are commercially available for micro-emulsification, including Shirasu porous glass (SPG), polymeric, and micro-sieve membranes. Among them, the SPG membrane has been more popular as it can withstand high flow pressure and its availability for surface modification [7, 11]. SPG membranes, however, are expensive. The present research used an inexpensive commercially available syringe filter as the membrane template, as a substitute for the SPG membrane, to set up a W/O/W double emulsion system. This modification can not only reduce production cost and time but also can produce MCs within a narrow size range, which is very desirable for uniformly dispersing them in the resin. More importantly, different morphologies or shapes of MCs, including elongated ones, can be produced by manipulating parameters such as pump rate and pore sizes of the syringe filters. Elongated MCs increase the probability of the MCs being in the path of the microcracks as well as enhance MC/resin adhesion [12, 13]. Both these factors can potentially boost the self-healing efficiency.

Polyvinyl alcohol (PVA) has been widely used as a stabilizer in emulsion systems. However, it has also been studied as a 'link' connecting MCs with resins and increasing the MC/resin interaction [14]. The hydrocarbon part (CH_2CH) of the PVA can get attached to the PLGA shell via hydrophobic interactions while the hydrophilic (OH) region extends into the SPI resins, boosting the MC/resin interfacial interaction [14]. Earlier, it was shown that the combination of the PVA-aided hydrogen bonding on the surface of the SPI-PLGA MCs and the elongated MCs creates a positive impact on both the self-healing performance and the mechanical performance [12]. In the present study, SPI-containing PLGA MCs were produced using a syringe-filter via membrane emulsification technique. The process delivers high encapsulation efficiency and allows producing size-tunable MCs. Both spherical and elongated MCs with aspect ratios of up to 20 were prepared and used to create self-healing soy protein-based resins. Both spherical and elongated MCs resulted in self-healing efficiencies of over 40%. While elongated MCs reinforced the resin, spherical MCs reduced the mechanical properties.

Materials and methods

Materials

Soy protein isolate (SPI), ProFam 974, was provided by Archer Daniels Midland Company, Decatur, IL. Poly (DL-lactide-co-glycolide) (50:50, ester-terminated PLGA) was purchased from the Division of DURECT Corporation, Birmingham, AL. Two inherent viscosities of 1.15 dL/g and 1.20 dL/g of PLGA in hexafluoroisopropanol were obtained depending on their availability. Both worked equally well and were used interchangeably. Poly (vinyl alcohol) (PVA, average Mw 31,000–50,000, 98–99% hydrolyzed), sodium hydroxide pellets (NaOH, 97.0%), glutaraldehyde (GA, 25 wt% solutions in water), ethyl acetate (EA, ≥99.8%), and polyvinylpyrrolidone (PVP), Rhodamine B (powder) and Bradford reagent (0.1%), Coomassie blue R-250 solution (composed of 45% methanol, 10% acetic acid and deionized (DI) water in the ratio 5:4:1) and sodium dodecyl sulfate (SDS) were purchased from Sigma-Aldrich (St. Louis, MO).

Preparation of MCs

The present research used a W/O/W double emulsion method to prepare microcapsules [4]. SPI/water solution, the healant, was encapsulated in PLGA shells. To prepare the healant, 100 mL of SPI/water solution (0.15 g/mL) was denatured using 10 mL of a 4 M NaOH solution at 80°C and 300 rpm for 15 min. Prepared SPI solution (10 mL), healant, and separately prepared PLGA/EA solution (30 mL, 0.01 g/mL) were stirred at the highest power of the vortex mixer (BenchMixer) for 10 min to form a W/O inverted emulsion. As explained below, MCs with two morphologies, spherical and elongated, were produced.

Producing spherical MCs using the syringe-filter method (abbreviation: SF-I)

The prepared W/O emulsion was then extruded through a 0.45 µm-syringe filter and a 25-gauge 50-mm needle using a dual-syringe pump (PHD ULTRA, Harvard Apparatus, MA, USA) at the rate of 3 mL/min into 80 mL of 5 wt% PVA/water solution while being stirred. The experimental set-up for making MCs is shown in Fig. 1 (top right part). The entire mixture was stirred at 300 rpm at room temperature (RT) during the extrusion. The mixture was kept stirring overnight to allow complete evaporation of EA, and the MCs that formed were collected by centrifuging the mixture at 5000 rpm (Thermo Scientific Super-Nuova) for 10 min. The MCs were washed with deionized (DI) water twice before freeze-drying at -82°C for 24 h.

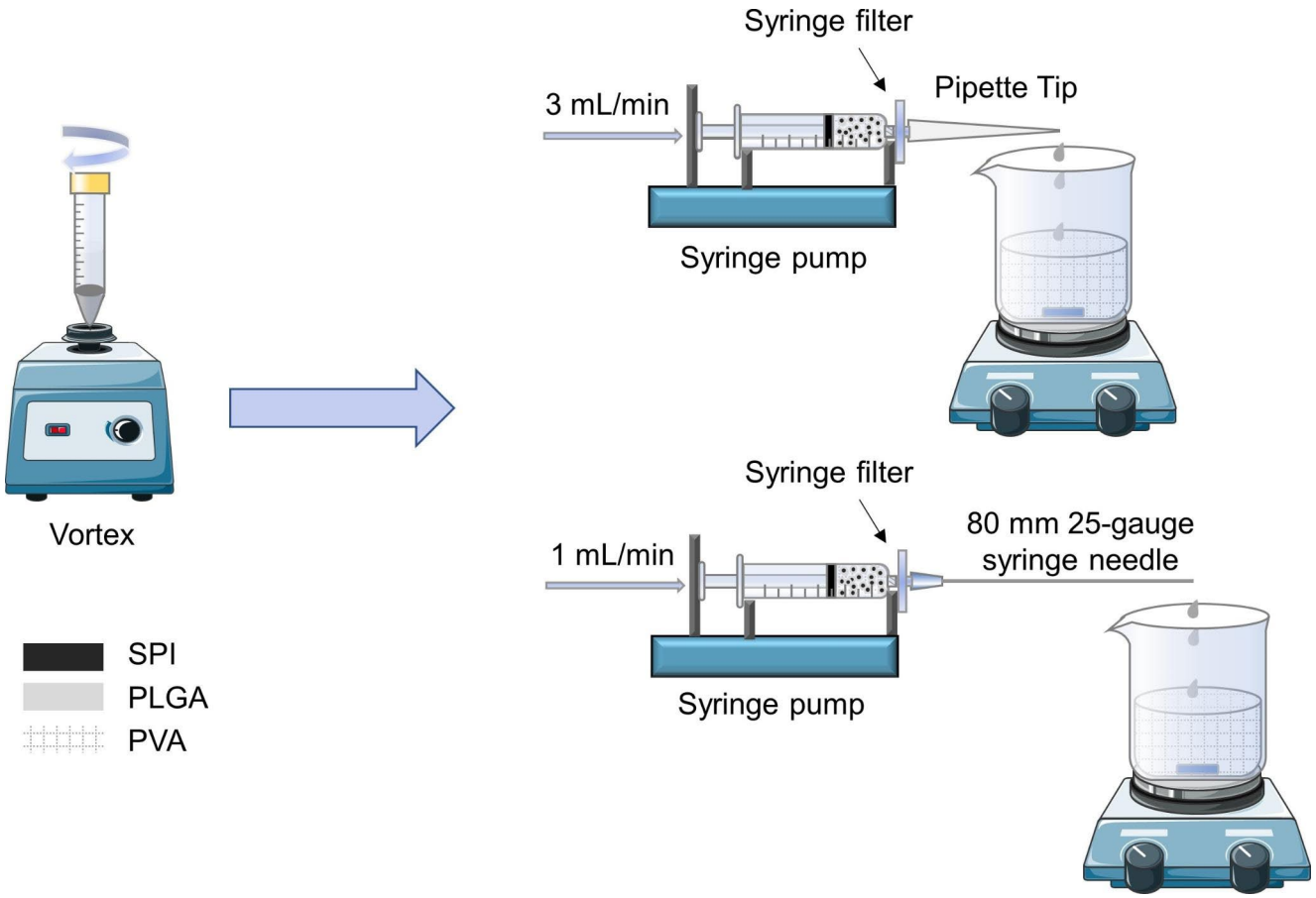

Fig. 1 Experimental set-up for making MCs

Producing elongated MCs using the syringe-filter method (abbreviation: SF-II)

Elongated MCs were produced in a slightly different way from spherical MCs. As is shown in Fig. 1 (bottom right part), a 25 gauge, blunt-end, 80 mm long needle was used to generate the elongated MC shapes. The W/O emulsion was pumped (extruded) at the rate of 1 mL/min into a 200 mL glass beaker containing 80 mL of 5 wt% PVA water solution. The entire mixture was stirred at 300 rpm at RT during the extrusion. The mixture was kept stirring overnight to fully evaporate the EA, and the elongated MCs were collected by centrifuging the mixture at 5000 rpm for 10 min. The MCs were washed with DI water twice before freeze-drying at -82°C for 24 h. Elongated MCs were assumed to be formed while traveling along the 80 mm long path of the 25-gauge needle.

Preparation of SPI-based self-healing green resins

Self-healing green resins were prepared simply by mixing denatured SPI/water solution and different amounts of MCs and crosslinking the SPI using GA. Briefly, 10 g of SPI powder was dissolved and denatured in 8% NaOH solution for 15 min. The SPI solutions were then blended with desired loadings of MCs (0, 5, 10, 15, 20, 30 wt% of SPI powder), separately, 10 min before adding 20 wt% of GA crosslinker. Twenty minutes later, the solution was poured into Teflon® coated molds and cured overnight in the oven at 75°C in the form of sheets. To obtain fully crosslinked SPI resin sheets, they were hot-pressed using a Carver hot-press (Carver Inc., Model No. 3895.4NE0000, Wabash, IN) with a set pressure at 0.09 MPa at 80°C for 10 min. Spacers of 1 mm thickness were used to obtain uniform thicknesses of the SPI resin sheets. Resin specimens for self-healing efficiency tests were cut into the desired shape as per ASTM E647-08 [15], as shown in Fig. 2**(a)** [12]. Specimens were kept in a desiccator to prevent additional moisture absorption for three days before performing self-healing efficiency tests.

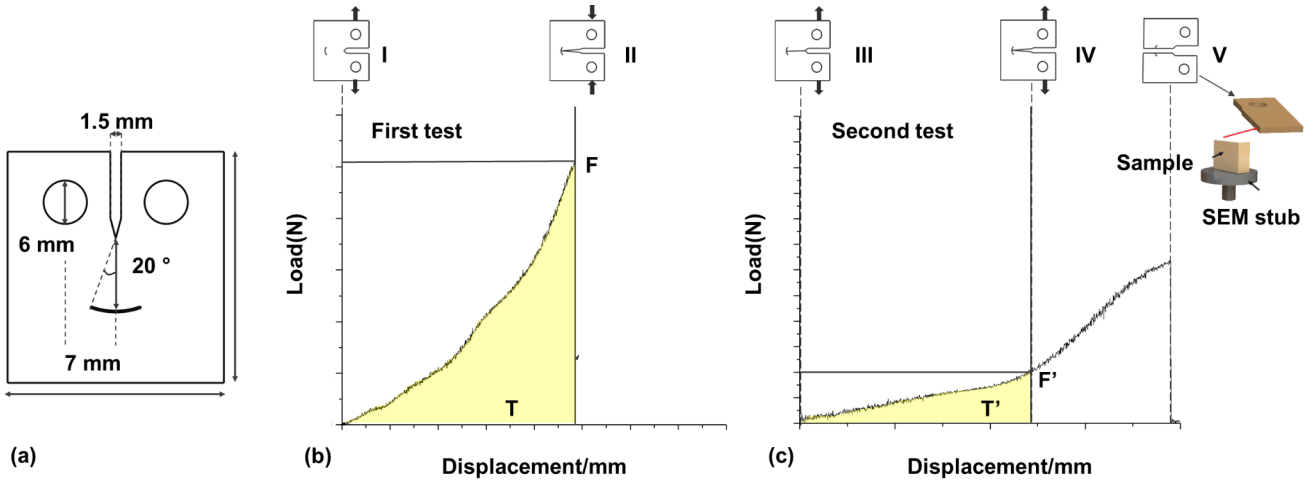

Fig. 2 (a) Self-healing test specimen geometry; (b) and (c) load vs. displacement plots obtained during typical self-healing tests [12]

Characterization of the MCs

Scanning electron microscope (SEM) analysis

SEM (Leo 1550 SEM and Zeiss Gemini 500 FESEM) was used to characterize the shapes, sizes, morphologies, and surface topographies of MCs. To prepare specimens for SEM study, MCs were resuspended in water, and a drop of the suspension was deposited on a conductive carbon tape that was glued to the SEM stub and dried before being coated with gold.

Evaluation of protein loading in MCs

Protein loading in the MCs was determined using the protocol reported by Hora et al. [16]. Briefly, MCs (100 mg) were milled into powder to release the SPI slurry, and the powder was added to 10 mL of 10 mM NaOH, which contained 5% (w/v) SDS. The suspension was centrifuged at 5000 rpm for 10 min to discard the insoluble residue. A standard calibration curve was set up using a series of standard SPI solutions. SPI solutions were prepared with concentrations ranging from 10 mg/mL to 0.1 mg/mL using a ten mM NaOH solution. Then a desired amount of the Bradford agent was added to all standard SPI solutions and samples (pH = 2, 0.5 mM HCl adjusted), respectively, until a blue color was observed. The protein loading was calculated at the maximum absorption at 595 nm using a UV/Vis spectrophotometer (Perkin-Elmer Lambda 35) [16].

Confocal laser scanning microscopy (CLSM)

CLSM (Zeiss LSM 710) was employed to analyze the core-shell structure and to confirm the presence of SPI inside the MCs. The SPI slurry was dyed using Rhodamine B water solution (1 wt%) before emulsification. MCs were prepared using the same process described above in Sect. 2.2. A 63X oil-immersion lens and the associated filter (514 nm wavelength excitation) were used to characterize MCs.

Attenuated total reflection–Fourier transform infrared (ATR-FTIR) spectroscopy

ATR-FTIR (Magna 560, Nicolet Instrument Technologies, Fitchburg, WI, USA) with split pea accessory was used to analyze SPI-PLGA MC chemical content. Each sample batch was scanned from 4000 cm^{-1} to 500 cm^{-1} with three repeats to assure data integrity.

Characterization of self-healing SPI resins

SEM characterization

Fracture surfaces of resin specimens fractured during the tests were characterized using SEM after mounting them vertically on double-sided conductive carbon tapes glued to the metal stub, as shown in Fig. 2**(c)** [12].

Tensile characterization

The stress vs. strain plots were obtained using an Instron universal tester (Instron, Model 5566). For tensile testing, resin specimens were cut carefully into strips with dimensions of 50 mm × 10 mm × 1 mm using a shear cutter. The gauge length and crosshead speed for tensile tests were set to 30 mm and 3 mm/min (0.1 min^{-1} strain rate), respectively. All specimens were kept at ASTM conditions of 21°C and 65% relative humidity (RH) for three days prior to conducting the tests. Fracture stress, fracture strain, and Young's modulus values were obtained from the plots.

Self-healing efficiency tests

As shown in Fig. 2(b) and (c), the self-healing efficiency tests were conducted in five steps: (I) mounting specimens on Instron; (II) pulling the specimen to create a 10 mm crack in the specimen (up to the mouth-shaped arc); (III) removing specimens from Instron, pressing the edges of the crack back together and allowing specimens to heal for 24 h in a sealed container; (IV) remounting the healed specimens in Instron and pulling them to reopen the 10 mm crack; (V) continuing to pull until the specimen breaks into two pieces. The crosshead speed for these tests was set at 0.3 mm/min, the same as before, as per ASTM E647-08 [15].

Self-healing efficiency of the resin was defined as the ratio of the fracture toughness of the healed resin and the virgin resin, as shown in Eqs. 1 and 2 [12, 17]. The F and F' correspond to the strength (resin failure load) in the first test (step II) and the second test (step V), respectively, at the same displacement, and T and T' correspond to the toughness (yellow areas under the test curve, shown in Fig. 2(b) and (c) [12]) in the first and the second tests, respectively, at the same displacement [12].

$$\eta_T = \frac{T' - T}{T} \times 100 \tag{1}$$

$$\eta_F = \frac{F' - F}{F} \times 100 \tag{2}$$

Results and discussion

Characterization of SPI-PLGA MCs

MC sizes and shell wall thicknesses were determined by randomly selecting MCs within the SEM images taken using Image J software.

Figure 3(a), (c), and (d) show SEM images of SF-I MCs obtained via the syringe-filter method. As can be seen, most MCs are spherical and intact, while a few are broken. The average diameter of MCs in this case (N > 150) was 1.30 µm ± 0.71 µm, and the diameters ranged between 0.44 and 5.71 µm and the shell thickness (N > 100) ranged between 0.1 and 0.25 µm. Figure 3(b) presents the histogram of the size distribution of SF-I MCs. It can be seen from the histogram that most MC diameters fall within a narrow range of 0.5 to 1.8 µm. A few sub-micrometer capsules (the smaller MCs) and a few broken MCs can also be seen. Typically, sub-micrometer capsules and broken MCs are undesirable in the preparation of MCs as they do not help the self-healing of the resin but can be detrimental to the mechanical properties of the resins if added.

Figure 4(a), (c), and (d) show typical SEM images of SF-II SPI-PLGA MCs prepared by the syringe-filter method. In this case, the MCs possess a wide range of aspect ratios (from 1 to 20) and a mix of distinctive shapes that include spherical, rod-like, dog-bone-like, and spindle-like. The highest aspect ratio observed from the SEM results was around 20. The elongated shapes were believed to have been a result of the 80 mm long needle used in the MC preparation process, as shown in Fig. 1. As observed by previous researchers, MCs with elongated shapes have the potential to store more healing agents and enhance self-healing efficiency [12, 13]. In addition, their longer length increases the probability of them being in the path of the microcracks and, hence, can be expected to result in higher self-healing efficiency. It is also possible that elongated MCs can act as reinforcement to improve the mechanical properties of a resin, particularly if the shell has high strength and MC/resin bonding is good. However, a higher strength of the MC shell could also reduce the self-healing efficiency by preventing shells from fracturing and releasing the healant.

In terms of the shapes of the MCs, a large number of elongated MCs are present in the overall mix of the MCs in the SF-II sample (Fig. 4(a). An average diameter of 11.64 µm ± 5.01 µm (N > 200) was observed for this sample, which was almost nine times as large as those in the SF-I sample, which had an average diameter of 1.30 µm. The reason for larger MC is perhaps the combining of MCs along the needle pathway, as seen in CLSM images and discussed in the Sect. 3.3. Figure 4(b) shows the size distribution histogram of intact spherical MCs ranging from 5 to 15 µm, in length.

Protein loading analysis

Protein loading in SF-I was calculated to be 4.07 wt%, while in SF-II, it reached 10.02 wt%. One reason for this was that MCs in SF-II were much larger in diameter (11.64 µm) than those in SF-I (1.3 µm). It is known that the loading ratio of SPI-PLGA MCs cannot exceed the feeding ratio, i.e., the protein concentration of 13.67 wt% used [12].

Confocal laser scanning microscopy (CLSM)

Figure 5(a) and (b) show CLSM images of SPI-PLGA SF-I MCs in fluorescent and transmission modes, respectively. The yellow color in the MCs seen in Fig. 5(a) indicates the presence of SPI and hence, confirms that the MCs indeed contain SPI slurry. Both Fig. 5(a) and (b) further confirm the core-shell structure of the MCs.

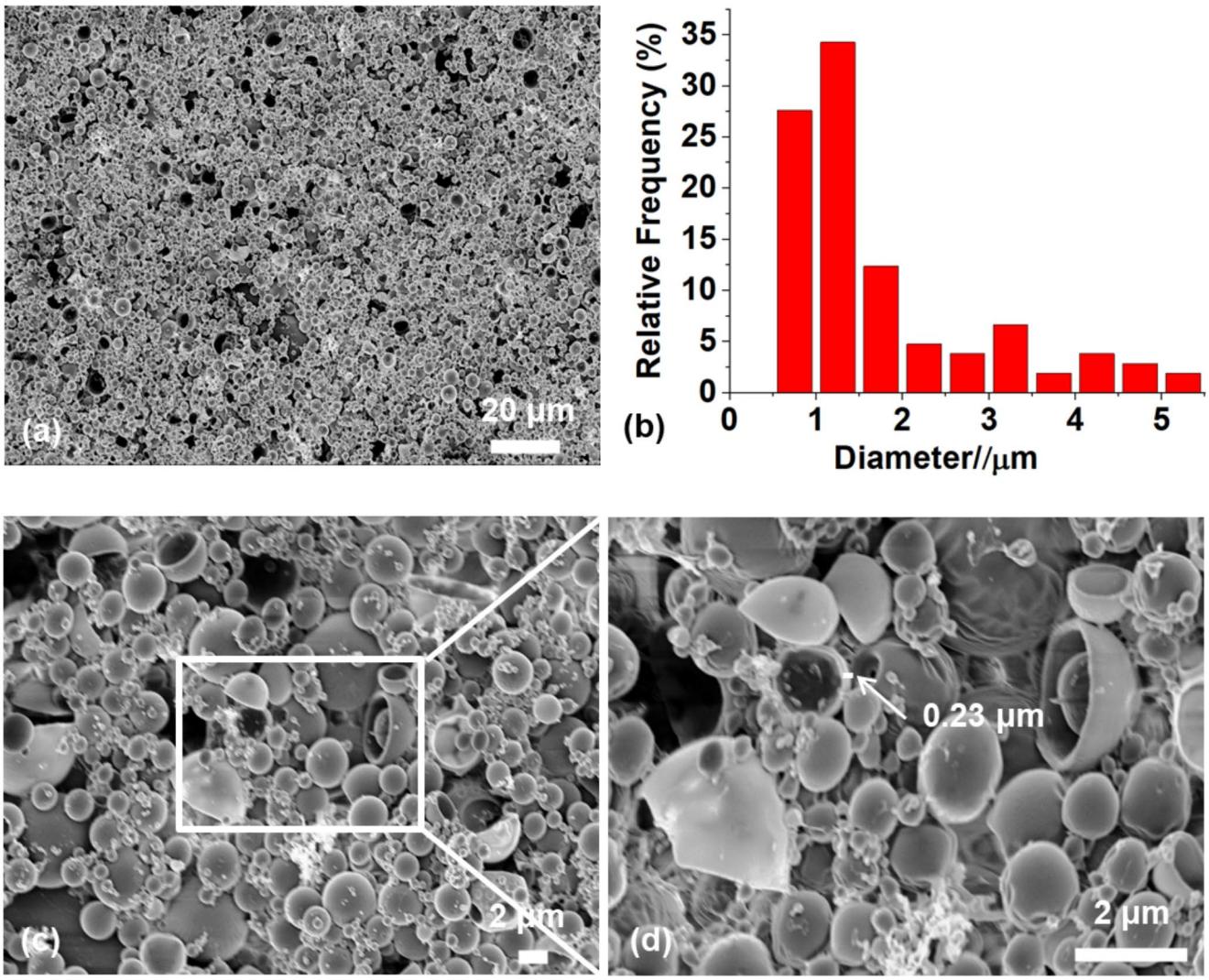

Fig. 3 SEM images of SF-I SPI-PLGA MCs obtained via the syringe-filter method: (a), (c) and (d) are typical images of MCs. Figure (b) shows the size distribution histogram of spherical MCs

Figure 6 presents CLSM images showing the internal structures of SF-II MCs. Figure 6(a) and (c) show fluorescent images of the MCs, while Fig. 6(b) and (d) show transmission images. From all images seen in Fig. 6, it can be confirmed that SF-II elongated MCs are loaded with SPI protein in spite of their different shapes. As seen in both images in the transmission mode (b) and (d), black dots can be seen inside some elongated MCs. These could either be smaller sub-MCs that get incorporated in the bigger MCs, or they could be air bubbles. Corresponding fluorescent images (a) and (c) show the contours of elongated MCs and confirm the existence of sub-MCs or air bubbles within the larger MCs. These results are similar to those reported earlier by Kim and Netravali [4].

ATR-FTIR analysis

Figure 7 shows spectra of PLGA, SPI, PVA, and prepared SF-I and SF-II MCs. Signature absorbance peaks of different functional groups are demonstrated by these ATR-FTIR spectra. For example, a distinguishable carbonyl (C = O) peak at 1725 cm^{-1} can be seen in the PLGA spectrum. Both SF-I and SF-II MCs show a strong peak at 1725 $cm^{-1,}$ indicating the presence of PLGA (shell) on the surfaces as can be expected [18]. Similarly, a peak belonging to bending vibration for the amine group (NH_2) from 1550 to 1650 cm^{-1} can be seen in SPI, SF-I, and SF-II spectra [19]. Spectra for PVA, SPI, SF-I, and SF-II MCs demonstrate an absorption peak at around 2900 cm^{-1} for the valence C-H vibration [20]. Furthermore, an aliphatic -CH_2- peak appears in PVA as well as in the spectra of SF-I and SF-II MCs at 750 to

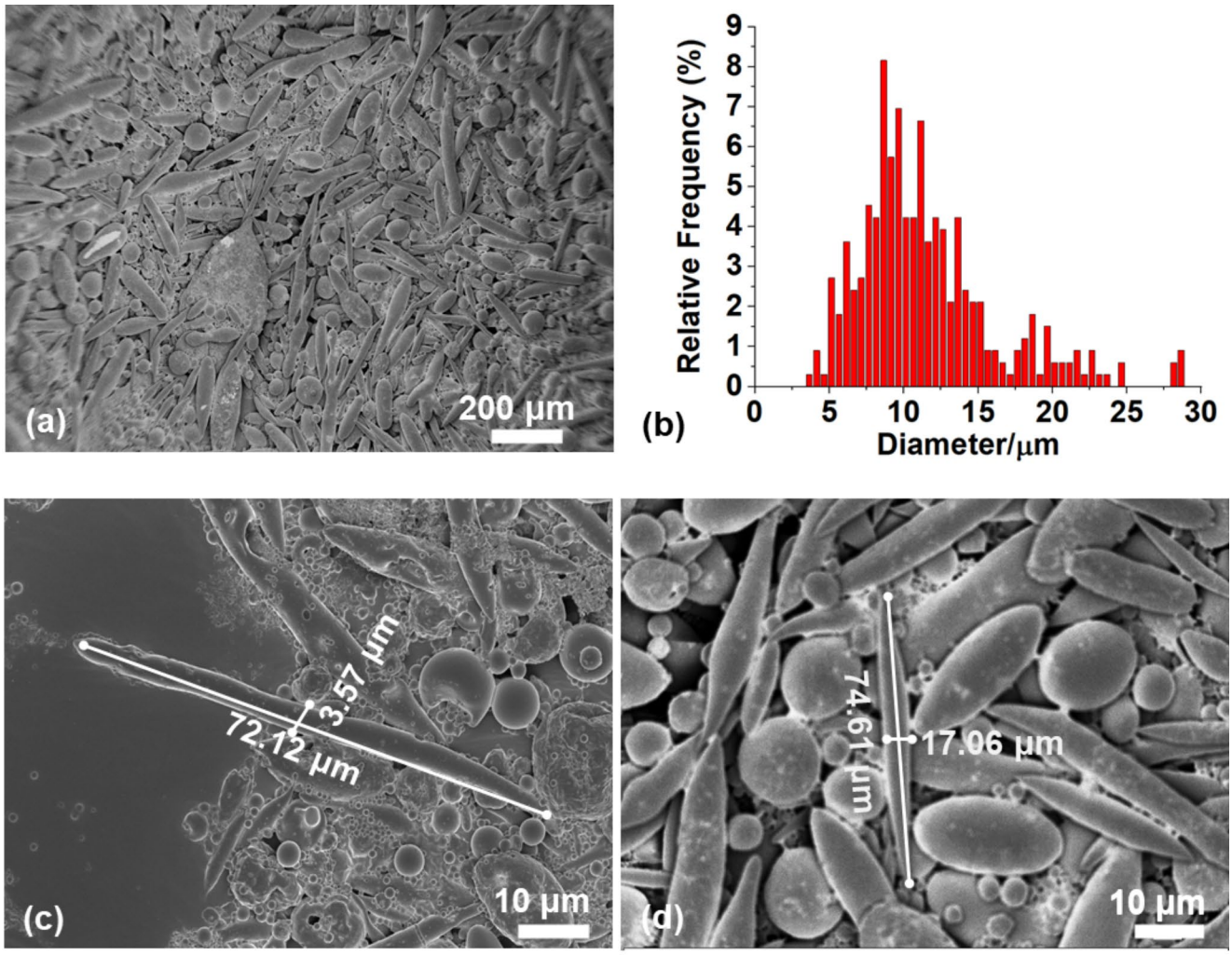

Fig. 4 SEM images of SF-II SPI-PLGA MCs (a, c and d) were obtained via the syringe-filter method. Figure (b) shows the size distribution histogram of the MCs

850 cm^{-1} [21]. These spectra confirm the presence of both SPI and PVA on the surfaces of SF-I and SF-II MCs.

SEM analysis

To demonstrate self-healing behaviors clearly, resins with the highest loading of MCs were tested for self-healing efficiency. Specifically, SPI resins loaded with 15 wt% SF-I MCs and 30 wt% of SF-II MCs were chosen to study their self-healing behavior.

Figure 8 shows typical SEM images of the microcracks, and fracture surfaces of resins loaded with 15 wt% spherical SF-I MCs. The released healant (SPI) is seen flowing out from SF-I SPI-PLGA MCs in both Fig. 8(a) and (b). While self-healing is accomplished mainly through microcrack healing, in this case, the amount of healant, SPI, seems insufficient to fill the microcrack. Filling the entire microcrack with the healant and bridging the fracture surfaces is critical for healing it. The volume between two fracture surfaces is overwhelmingly larger than the limited amount of healing agent available from the MCs. Since more healant is needed to fill the microcrack, it could be problematic to have a low loading, i.e., having a limited number of MCs in the resin. However, increasing the size (diameter) of MCs or having higher MC loading to obtain more healant, can reduce the mechanical properties of the resin, i.e., at the expense of the mechanical properties of the resin [4, 12]. Figure 8(c) shows the smooth surface of an unbroken SF-I spherical MC on the fracture surface, which suggests that the MC/resin bonding may not be strong enough. Spherical MCs, because of their smooth surface, may also be prone to easily debond from the resin at the microcracks rather than fracturing. While PLGA is hydrophobic, having low surface energy, SPI resin is hydrophilic, having high surface energy, and it is possible that the bonding is not as desired.

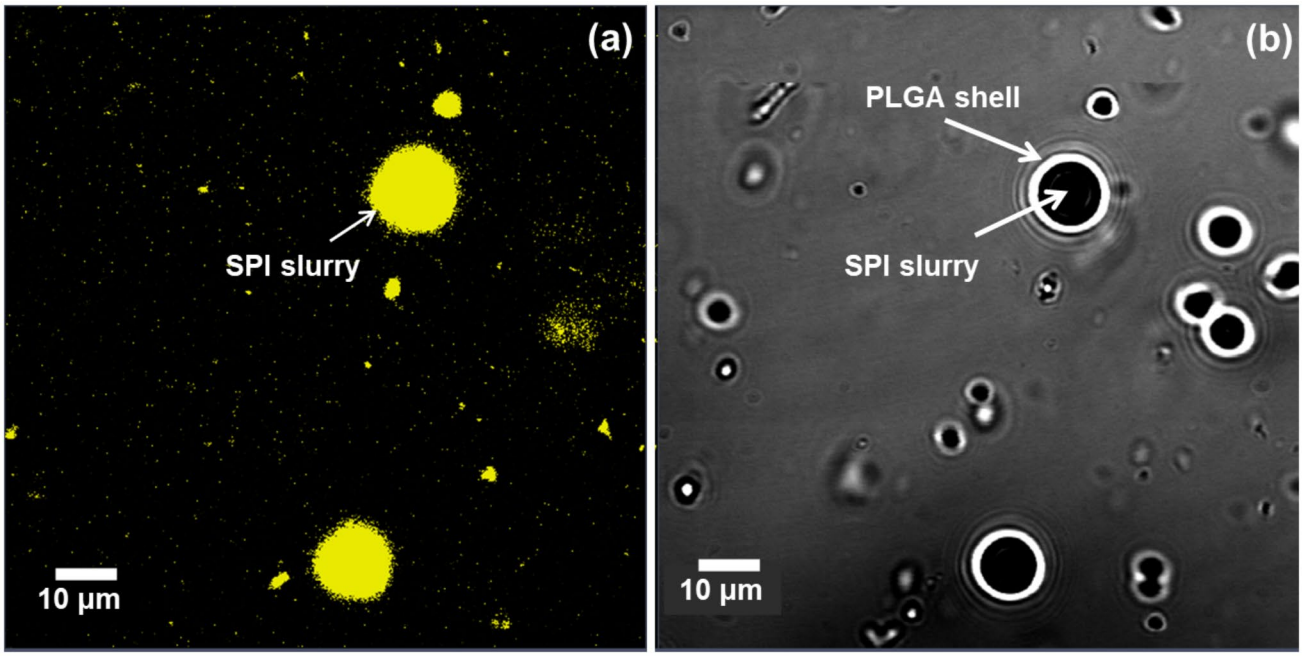

Fig. 5 CLSM images showing the morphologies of SPI-PLGA SF-I MCs (a) fluorescent image and (b) image in transmission mode. The yellow color in the fluorescent image indicates the protein content

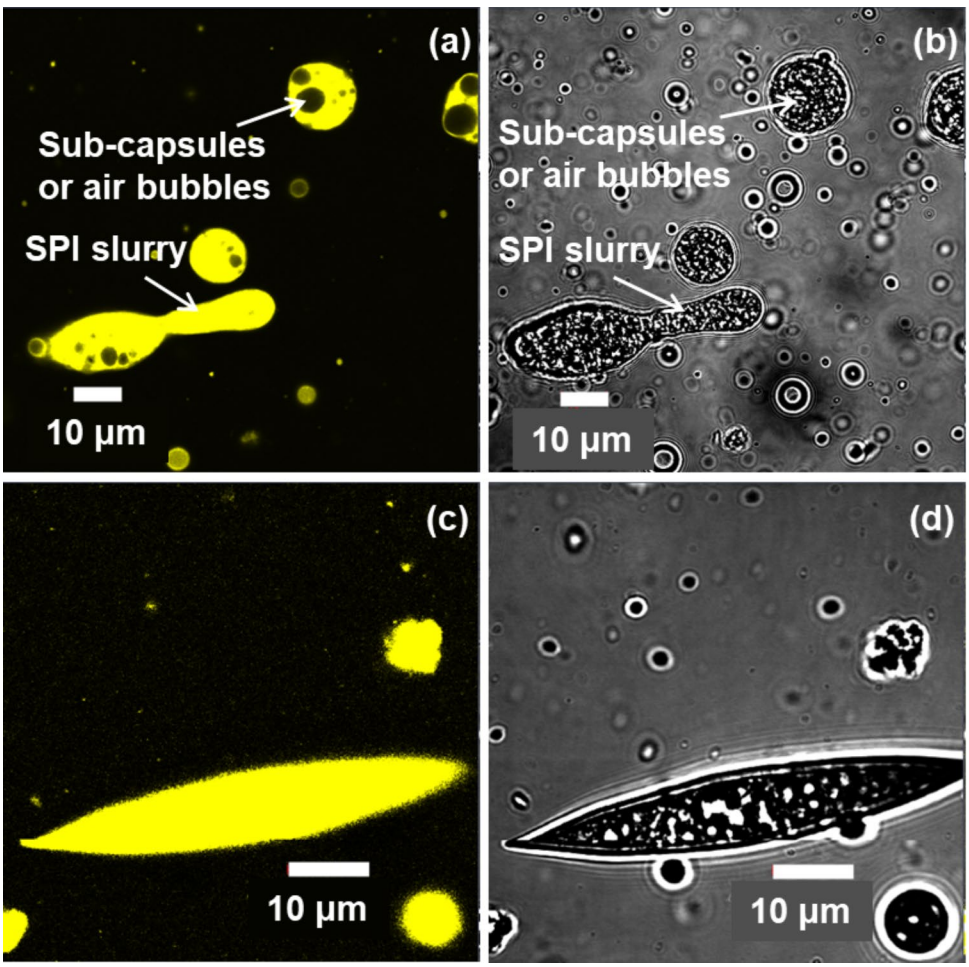

Fig. 6 CLSM images showing the internal structures of elongated SPI-PLGA SF-II MCs: (a) and (c) are the fluorescent images and (b) and (d) are the images of MCs taken in transmission mode by CLSM. The yellow color indicates protein (mostly)

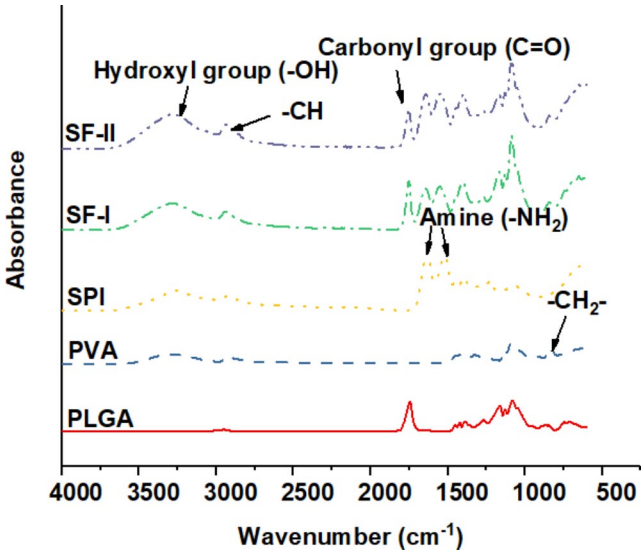

Fig. 7 ATR-FTIR spectra of MCs, compared with PLGA, PVA, and SPI

Figure 9 displays typical SEM images of microcracks and fracture surfaces in resins loaded with 30 wt% of SF-II MCs. Many bridges between the two fracture surfaces can be identified in Fig. 9(a) to (c) with different crack sizes where the healant has burst out as a result of MCs being fractured by the advancing microcracks. The crosslinking of the healant happens quickly once it gets in contact with the excess GA present in the resins. The elongated MCs were designed to store more healing agent and enhance the mechanical performance of resins. However, as stated earlier, with higher aspect ratios, elongated MCs also increase the probability of being in the path of the microcracks, assuring their fracture and, thus, increasing the self-healing efficiency [12, 13].

Figure 9(d) demonstrates a resin failure mode in which a microcrack propagates within the resin along the outer edge of an elongated MC without fracturing it. This failure mode can occur when the microcracks run along the length, rather than across the MCs. While the MCs are randomly

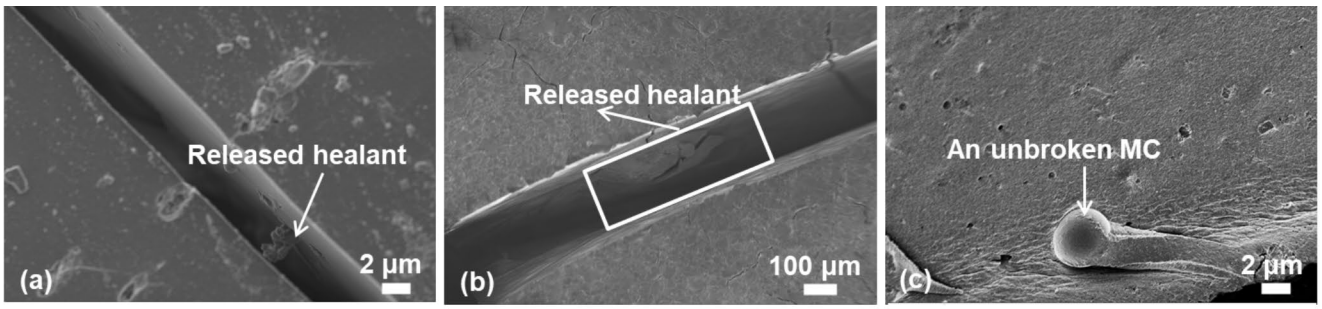

Fig. 8 Typical SEM images of the fracture surfaces of SPI resins loaded with 15 wt% SF-I SPI-PLGA MCs

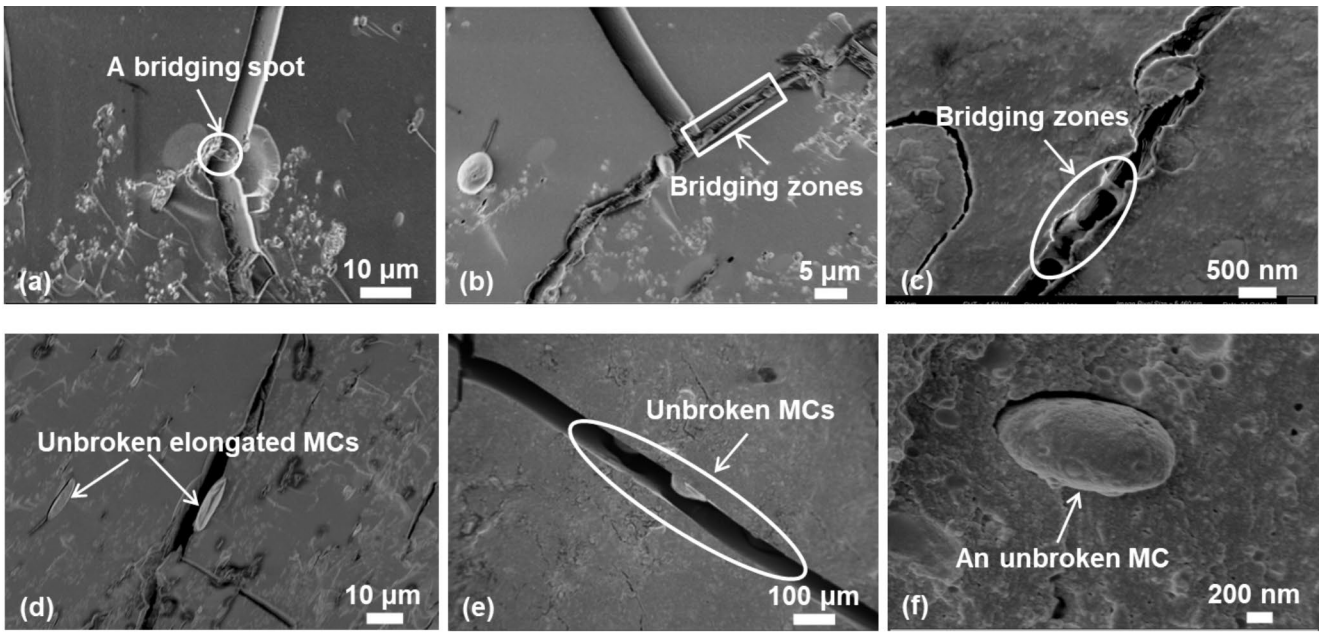

Fig. 9 Typical SEM images of the fracture surfaces and crack sizes of SPI resins loaded with 30 wt% of SF-II SPI-PLGA MCs

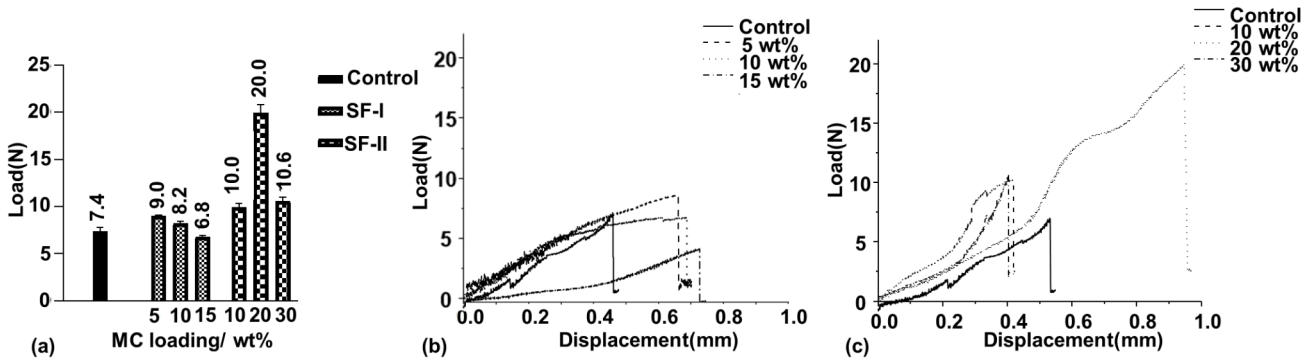

Fig. 10 (a) Effect of MC loading on resin failure load in self-healing efficiency tests. Typical load vs. displacement plots for (b) resins with SF-I MCs and (c) resins with SF-II MCs

oriented within the resin, such situations can result in lower self-healing efficiency and compromise the mechanical performance of the structural composites. From Fig. 9(d), one can conclude that the MC/resin interfacial bonding was insufficient to withstand the shearing at the MC/resin interfacial boundaries. Similar situations can be seen in Fig. 9(e) and (f). A small gap between the healant and the MC shell observed in the SEM image shown in Fig. 9(f) confirms weak MC/resin bonding. Bucknall et al. illustrated this phenomenon by using rubber particles as fillers to reinforce the nylon matrix. They revealed the dilatation in nylon matrix as a result of the formation of cavities around reinforcement fillers which accelerated shear yielding [22].

Mechanical properties

A two-tailed unequal variance t-test was utilized for statistical analysis, and a 95% confidence interval was chosen. Tests were performed five times to confirm experimental reproducibility. Data for failure load are shown as a histogram of means ± standard deviation.

The effect of SF-I and SF-II MC loading on the resin failure load (an indicator of strength) during the self-healing efficiency tests are depicted in Fig. 10(a), and typical load vs. displacement plots for each sample are shown in Fig. 10(b) and 10(c). The resins showed that there is an optimal MC loading (wt%) beyond which the strength of the resin drops, which is similar to what was observed by earlier researchers for the soy protein-based resin [4, 5, 12]. They suggested that at higher loadings, MCs start to aggregate, forming significant defects which affect their tensile properties. From Fig. 10, it can be concluded that resins loaded with SF-I MCs showed minor enhancement in the failure load of the resins at a low loading of 5%. Additional MC loading, however, reduced the failure load (strength), i.e., the overall mechanical performance of the resin. As can be seen in Fig. 10(b), resins with SF-I MCs showed increased displacement and reduced load at break with increased MC loading, suggesting that addition of spherical MCs reduces the strength and increases the ductility of the resin. The load at break of resins with SF-II MCs showed a marked enhancement at 20 wt% MC loading. Additional MC loading led to a decrease in resin strength. The results illustrate a fact that spherical MCs tend to improve the mechanical properties only at low MC loading. Earlier results suggested that adding any MCs decreases the resin strength [4, 5, 13]. From Fig. 10(c), it can be observed that the resin with 20% MC loading demonstrated load at the break with very high displacement, indicating a more ductile material. Lapčík et al. have reported similar results [23]. Therefore, it was assumed that an optimal addition of self-healing MCs can boost the ductility of resins. These results are consistent with the SEM analysis (shown in Fig. 9), which showed small cavities around intact MCs or exposed the intact MCs on the fracture surfaces indicating poor bonding of spherical SF-I MCs which can compromise resin mechanical properties. The strength enhancement obtained in resins loaded with SF-II may result from their elongated shapes.

Figure 11 depicts the effect of different MC loadings on the toughness of resins in self-healing efficiency tests. Toughness, for comparative purposes, was calculated as the area under the curve. Resins loaded with SF-I MCs showed a minor enhancement in toughness at all loading levels. In contrast, resins with SF-II MCs greatly improved the toughness at 20 wt% loading compared to the control (0 wt% loading). Toughness has been shown to increase by 8–10 folds in fiber-reinforced composites when cracks run parallel to fibers and result in fiber/resin debonding [24]. The elongated MCs (SF-II) may be comparable to fibers to some extent and provide an energy-absorbing mechanism through MC/resin debonding, leading to toughness enhancement. Earlier research indicated that a rougher fracture surface of resins with SF-II MCs compared to resins with SF-I MCs indicated a toughness effect, as shown in SEM images in Figs. 8 and 9 [25].

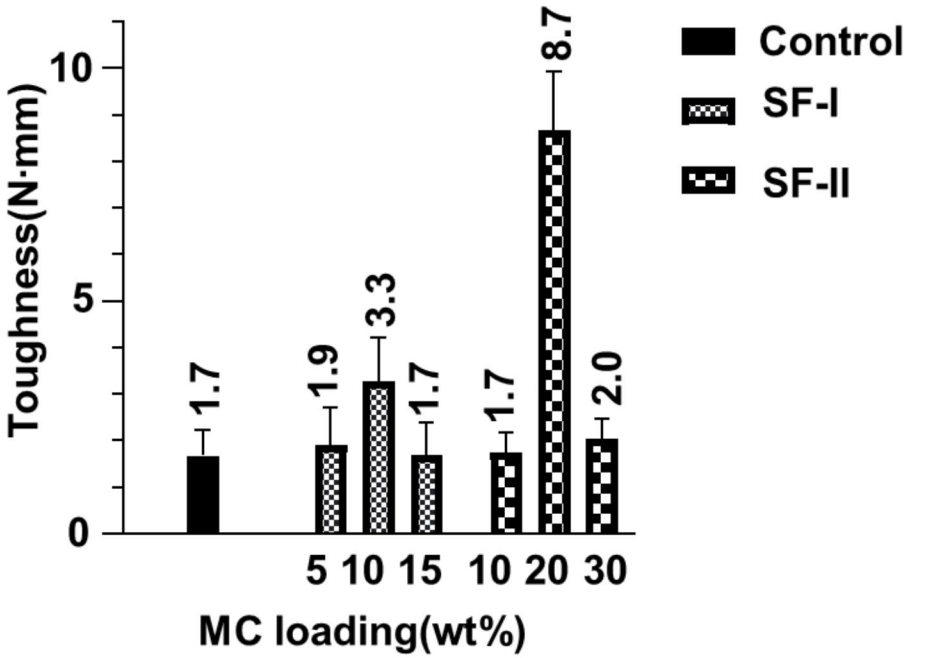

Fig. 11 Effect of MC loading on the resin toughness in self-healing efficiency tests

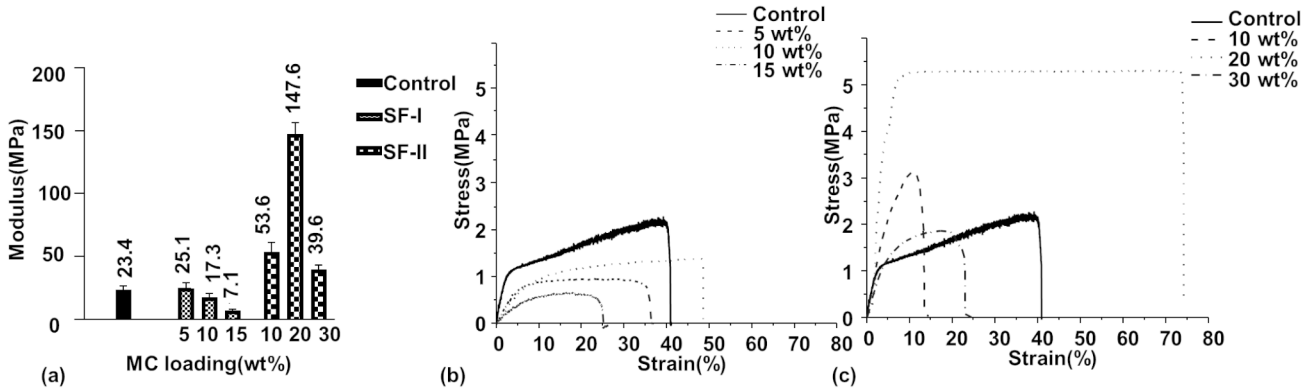

Fig. 12 (a) Effect of MC loading on the resin modulus values obtained from the tensile tests. Typical strain vs. stress plots in tensile tests with different MC loadings for (b) resins with SF-I MCs and (c) resins with SF-II MCs

Figure 12 presents the effect of MC loading on resin modulus values obtained from the tensile tests. Resins loaded with spherical SF-I MCs decreases in Young's modulus values at low loadings. The modulus dropped from 25.14 MPa to 7.1 MPa, when MC loadings increased from 5 wt% to 15 wt%. These results suggest, indirectly, that SF-I MCs may not be bonded well with the resin and are more likely to reduce the resin stiffness. Resins embedded with SF-II MCs reached a maximum Young's modulus value of 147.6 MPa with 20 wt% loading. The modulus, however, sharply decreased beyond 20 wt% MC loading. A possible explanation for this result is that overloaded MCs lead to aggregation at some locations. In the stress vs. strain plots shown in Fig. 12(b) and (c), it was noticed that the initial cracks propagated and eventually led to specimen failure as stress increased. In SF-I MC embedded resins, the fracture strains dropped as the MC loading increased, indicating that spherical MC loadings possibly introduced more defects, perhaps due to aggregation. This higher defect density contributed to the premature failure of samples. It is also possible that spherical MCs do not bond well to resin. The stress vs. strain plots of SF-II MC containing resins showed similar characteristics but higher modulus as well as higher fracture strains. For SF-II MC embedded resins, there was an optimum loading of MC (20%) that yielded resins with the highest fracture strain in the range of 70%. It can be

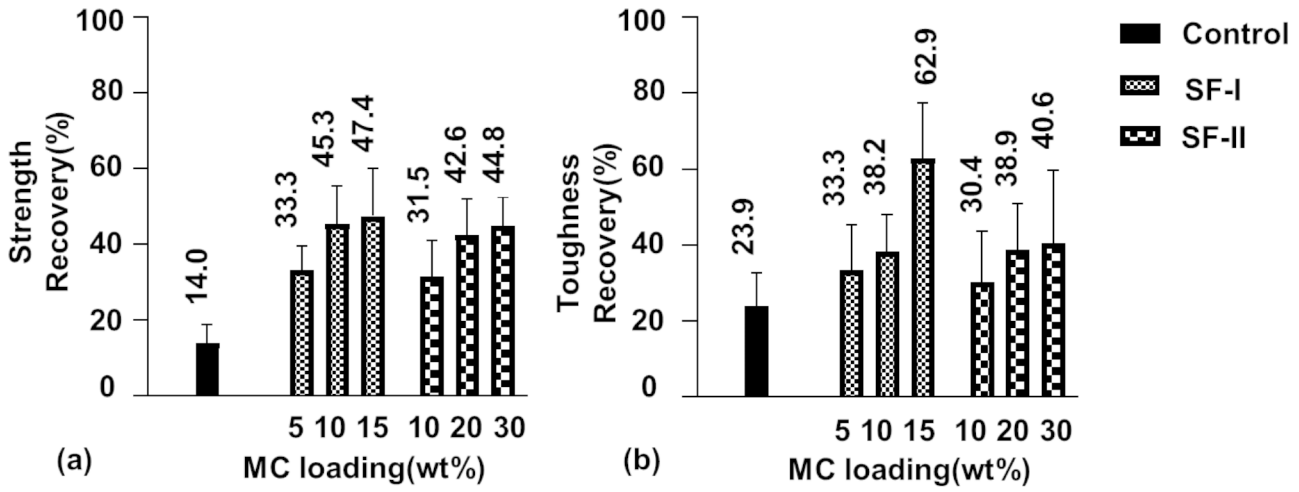

Fig. 13 Self-healing efficiencies of SPI resins as a function of MC loadings: (a) self-healing efficiency based on strength recovery (resin failure load); (b) self-healing efficiency based on toughness recovery

assumed that randomly distributed elongated MCs increase fracture strains as resins and MCs deform simultaneously and resin deformation around elongated MCs so that resin sustains stress till it reaches the fracture limits [25]. In any case, it is clear that additional MCs beyond the optimum loading compromise the resin's properties.

Self-healing efficiency tests

Figure 13 presents the self-healing efficiencies of SPI resins in terms of strength recovery as well as toughness recovery for both resins containing SF-I and SF-II MCs and as a function of MC loadings. As can be expected, resins with higher MC loadings resulted in higher self-healing efficiency for both SF-I and SF-II MCs. Resins loaded with 15 wt% of SF-I MCs displayed the highest self-healing efficiency for strength recovery of 47.4% compared to 14.0% for virgin resin (without MCs) and 62.9% toughness recovery compared to 23.9% for virgin resin. In the case of SF-II MCs, the self-healing efficiency for strength recovery reached 44.8%, and toughness recovery reached 40.6%. While self-healing efficiencies for resins with SF-I MCs are higher than resins containing SF-II MCs, this seems to be an artifact that results from the severely compromised mechanical properties of the resins containing SF-I MCs (as shown in Figs. 10 and 11). It was seen in Fig. 10 that the failure loads were significantly lower for resins containing SF-I MCs compared to those containing SF-II MCs. Also, Fig. 11 showed clearly that the toughness and modulus of resins with SF-I MCs were lower than those containing SF-II MCs.

The purpose of self-healing functionality is to recover the mechanical properties of the material by healing or bridging the microcracks that develop under stress to a level equivalent to or even higher than their virgin values without compromising their properties as a result of MC addition. Considering what has been discussed above, it seems that spherical SF-I MCs act as defects in the resins and degrade their mechanical properties, particularly at higher loadings. As a result, it can be concluded that SF-I MCs may not be suitable as self-healing fillers in this case. Resins with SF-II MCs, presented in Fig. 13, showed a slight improvement in self-healing efficiency between MC loadings of 20 wt% (42.6%) and 30 wt% (44.8%) in terms of strength recovery, and 38.9% and 40.6%, for corresponding MC loadings, in terms of toughness recovery. Compared with other soy self-healing soy protein-based resins, an earlier study by Kim and Netravali had shown a self-healing efficiency of up to 48% but with declined mechanical properties [4]. Self-healing efficiencies obtained in this study are in the same ballpark. Starch-based self-healing resins, on the other hand, have shown up to 66% strength recovery [5]. Apart from soy protein-based resins, 72% fracture stress recovery has been reported in the case of zein resins [13]. With the aid of 3D printing technology, Sanders et al. fabricated PMMA-filled MCs containing UV-curable resin that showed 87% recovery of the initial critical toughness [26]. Compared with the recovery self-healing efficiencies of conventional composites developed by other research teams, research on self-healing green composites is still in its infancy. Future direction should be directed to improving the resin/MCs interfacial bonding and obtaining higher aspect ratios of MCs that would yield higher self-healing efficiencies.

Conclusions

The use of the syringe-filter method resulted in a monomodal distribution of spherical SF-I MC diameters. However, SF-I MCs compromised the mechanical strength of the resins, possibly because of the weak MC/resin adhesion and spherical shapes. The self-healing efficiencies for resins containing SF-I MCs (15% loading) were 47.4% and 67.9% in terms of strength recovery and toughness recovery, respectively. However, these high numbers were a result of weakening of the resin. SF-II MCs containing elongated shapes were also produced using the syringe-filter method and turned out to be helpful in terms of mechanical reinforcement of the resin. The aspect ratios of elongated SF-II MCs reached as high as 20. MCs with high aspect ratios were dually beneficial as they could act not only as healing elements but may also reinforce the resin. SF-II MC containing resins (20% loading) reached high self-healing efficiencies at 44.8% and 40.6% in terms of strength recovery and toughness recovery, respectively. It is recommended that the application of self-healing fillers with high aspect ratios and good MC/resin bonding would bring great benefit to the development of self-healing materials. Self-healing green resins could enhance the durability of green composites and help in replacing petroleum-based conventional composites.

Acknowledgements The use of the Cornell Center for Materials Research Shared Facilities, which are supported through the NSF MRSEC program (DMR-1719875), is acknowledged. Authors would also like to acknowledge the funding support of Tata Cornell Institute for materials used in this work.

Funding This study was partially funded by a grant from Tata Cornell Institute as stated above.

Declarations

Conflict of interest The authors declare that they have no conflict of interest.

References

1. Chemat F, Vian MA, Ravi HK (2021) Toward petroleum-free with plant-based chemistry. Curr Opin Green Sustainable Chem 28:100450. https://doi.org/10.1016/J.COGSC.2021.100450
2. García MC, Torre M, Marina ML, Laborda F (1997) Composition and Characterization of Soyabean and Related Products. Crit Rev Food Sci Nutr 37:361–391. https://doi.org/10.1080/10408399709527779
3. Kim JR, Netravali AN (2018) Self-Healing Green Polymers and Composites. Advanced Green Composites. John Wiley & Sons, Inc., Hoboken, NJ, USA, pp 135–185. https://doi.org/10.1002/9781119323327.ch7.
4. Kim JR, Netravali AN (2016) Self-Healing Properties of Protein Resin with Soy Protein Isolate-Loaded Poly(D.L-lactide-co-glycolide) Microcapsules. Adv Funct Mater 26:4786–4796. https://doi.org/10.1002/adfm
5. Kim JR, Netravali AN (2017) Self-healing starch-based 'green' thermoset resin. Polymer 117:150–159. https://doi.org/10.1016/j.polymer.2017.04.026
6. Mauldin TC, Kessler MR (2010) Self-healing polymers and composites. Int Mater Rev 55:317–346. https://doi.org/10.1179/095066010X12646898728408
7. Vladisavljević GT (2019) Preparation of microemulsions and nanoemulsions by membrane emulsification. Colloids Surf A 579:123709. https://doi.org/10.1016/J.COLSURFA.2019.123709
8. Dat Lai Q, Thuy Loan Huynh T, Thuc Trinh Doan N et al (2022) Particle size distribution and homogenisation efficiency in high-pressure homogenisation of wheat germ oil-water system. Int J Food Sci Technol. https://doi.org/10.1111/IJFS.15760
9. Taha A, Hu T, Zhang Z et al (2018) Effect of different oils and ultrasound emulsification conditions on the physicochemical properties of emulsions stabilized by soy protein isolate. Ultrason Sonochem 49:283–293. https://doi.org/10.1016/j.ultsonch.2018.08.020
10. Thompson KL, Mable CJ, Lane JA et al (2015) Preparation of pickering double emulsions using block copolymer worms. Langmuir 31:4137–4144. https://doi.org/10.1021/acs.langmuir.5b00741
11. Fu X, Ohta S, Kamihira M et al (2019) Size-Controlled Preparation of Microsized Perfluorocarbon Emulsions as Oxygen Carriers via the Shirasu Porous Glass Membrane Emulsification Technique. Langmuir 35:4094–4100. https://doi.org/10.1021
12. Shi S, Netravali AN (2021) Bacterial cellulose integrated irregularly shaped microcapsules enhance self-healing efficiency and mechanical properties of green soy protein resins. J Mater Sci 56:12030–12047. https://doi.org/10.1007/S10853-021-06066-Y
13. Souzandeh H, Netravali AN (2019) Self-healing of 'green' thermoset zein resins with irregular shaped waxy maize starch-based/poly(D,L-lactic-co-glycolic acid) microcapsules. Compos Sci Technol 183:107831. https://doi.org/10.1016/j.compscitech.2019.107831
14. Murakami H, Kobayashi M, Takeuchi H, Kawashima Y (1999) Preparation of poly(dl-lactide-co-glycolide) nanoparticles by modified spontaneous emulsification solvent diffusion method. Int J Pharm 187:143–152. https://doi.org/10.1016/S0378-5173(99)00187-8
15. ASTM E647-00 Standard Test Method for Measurement of Fatigue Crack Growth Rates (2020) (n.d.). https://www.astm.org/DATABASE.CART/HISTORICAL/E647-00.htm
16. Hora MS, Rana RK, Nunberg JH et al (1990) Release of Human Serum Albumin from Poly(lactide-co-glycolide) Microspheres. Pharm Research: Official J Am Association Pharm Scientists 7:1190–1194. https://doi.org/10.1023/A:1015948829632
17. White SR, Sottos NR, Geubelle PH et al (2001) Autonomic healing of polymer composites. Nature 409:794–797. https://doi.org/10.1038/35057232
18. Paragkumar NT, Edith D, Six JL (2006) Surface characteristics of PLA and PLGA films. Appl Surf Sci 253:2758–2764. https://doi.org/10.1016/j.apsusc.2006.05.047
19. Combs JD (2016) Surface FTIR Techniques to Analyze the Conformation of Proteins/ Peptides in H2O Environment. J Phys Chem Biophys 6. https://doi.org/10.4172/2161-0398.1000202
20. Paniagua-Michel J, Fathepure BZ(2019) Microbial consortia and biodegradation of petroleum hydrocarbons in marine environments. In: Microbial Action on Hydrocarbons. Springer Singapore, pp 1–20https://doi.org/10.1007/978-981-13-1840-5_1
21. Prosanov IY, Matvienko AA (2010) Study of PVA thermal destruction by means of IR and Raman spectroscopy. Phys Solid State 52:2203–2206. https://doi.org/10.1134/S1063783410100318

22. Bucknall CB, Heather PS, Lazzeri A (1989) Rubber toughening of plastics. J Mater Sci 1989 24:6. https://doi.org/10.1007/BF02385450
23. Lapčík L, Maňas D, Lapčíková B et al (2018) Effect of filler particle shape on plastic-elastic mechanical behavior of high density poly(ethylene)/mica and poly(ethylene)/wollastonite composites. Compos Part B: Eng 141:92–99. https://doi.org/10.1016/J.COMPOSITESB.2017.12.035
24. Nikpur K, Chen YF, Kardos JL (1990) Fracture toughness of unidirectional short-fiber reinforced epoxy composites. Compos Sci Technol 38:175–191. https://doi.org/10.1016/0266-3538(90)90005-P
25. Guo P, Chen X, Gao X et al (2007) Fabrication and mechanical properties of well-dispersed multiwalled carbon nanotubes/epoxy composites. Compos Sci Technol 67:3331–3337. https://doi.org/10.1016/J.COMPSCITECH.2007.03.026
26. Sanders P, Young AJ, Qin Y et al(2019) Stereolithographic 3D printing of extrinsically self-healing composites. Scientific Reports 2019 9:1 9:1–6. https://doi.org/10.1038/s41598-018-36828-9